Nucl Eng Technol 47 (2015) 115–125

Available online at www.sciencedirect.com

ScienceDirect

journal homepage: http://www.journals.elsevier.com/nuclear-engineering-and-technology/

Original Article

RESIDUAL STRESS MEASUREMENT ON THE BUTT-WELDED AREA BY ELECTRONIC SPECKLE PATTERN INTERFEROMETRY

KYEONGSUK KIM [a], TAEHO CHOI [b], MAN GYUN NA [c], and HYUNCHUL JUNG [a,*]

[a] Department of Mechanical System Engineering, Chosun University, 309 Pilmun-daero, Dong-gu, Gwangju 501-759, Republic of Korea
[b] Department of Mechanical System Engineering, Graduate School, Chosun University, 309 Pilmun-daero, Dong-gu, Gwangju 501-759, Republic of Korea
[c] Department of Nuclear Engineering, Chosun University, 309 Pilmun-daero, Dong-gu, Gwangju 501-759, Republic of Korea

ARTICLE INFO

Article history:
Received 9 April 2014
Received in revised form
29 August 2014
Accepted 23 September 2014
Available online 21 January 2015

Keywords:
Butt-Welded Area
Elastic Modulus
Electronic Speckle Pattern Interferometry
Phase Difference
Residual Stress
Stress Distribution

ABSTRACT

Background: Residual stress always exists on any kind of welded area. This residual stress can cause the welded material to crack or fracture. For many years, the hole-drilling method has been widely used for measuring residual stress. However, this method is destructive. Nowadays, electronic speckle pattern interferometry (ESPI) can be used to measure residual stress with or without the hole-drilling method. ESPI is an optical nondestructive testing methods that use the speckle effect. Mechanical properties can be measured by calculation of the phase difference by the variation of temperature, pressure, or loading force.
Methods: In this paper, the residual stress on the butt-welded area is measured by using ESPI with a suggested numerical calculation. Two types of specimens are prepared. Type I is made of pure base metal part and type II has a welded part at the center. These specimens are tensile tested with a material test system. At the same time, the ESPI system was applied to this test.
Results: From the results of ESPI, the elastic modulus and the residual stress around the welded area can be calculated and estimated.
Conclusion: With this result, it is confirmed that the residual stress on the welded area can be measured with high precision by ESPI.

1. Introduction

Residual stress, or internal stress, is usually defined as the stress that remains in mechanical parts that exist in the bulk of a material without the application of an external load (including gravity), or other sources of residual stress, such as a thermal gradient [1]. They may be created by manufacturing processes such as casting, rolling, welding, heat treating, or forging, or may occur during the life of a structural or mechanical component [2,3]. The magnitude and

* Corresponding author.
E-mail address: yonggaryjung@gmail.com (H. Jung).

http://dx.doi.org/10.1016/j.net.2014.09.001
1738-5733/Copyright © 2015, Published by Elsevier Korea LLC on behalf of Korean Nuclear Society.

distribution of residual stresses are highly significant and need to be quantified since the mechanical behavior of different materials will be affected when they are present.

There are a number of different methods for measuring residual stress. These methods can be divided into two parts, the destructive method and the nondestructive method [4]. Hole drilling, ring coring, deep hole drilling, the slitting method, and the contour method can be included in the destructive method, whereas X-ray diffraction, neutron diffraction, magnetic method, ultrasonic method, and optical methods are included in the nondestructive method.

The hole drilling method is the most widespread technique for measuring residual stresses. This technique involves monitoring the strains generated by the relieved stresses when a small hole is drilled into a stressed material. These strains are usually measured by means of strain gage rosettes. However, it has some practical and economical drawbacks. For instance, the hole must be drilled in the center of the rosette since misalignments can cause significant errors. This method is also a destructive testing method.

The difficulty can be overcome using optical techniques. Among them, electronic speckle pattern interferometry (ESPI) is a technique that is very attractive in optical metrology not only for its noncontact nature but also for its relative speed. This is mainly due to the use of video detection and digital image processing [5,6]. The application of digital techniques in ESPI allows the automation of the data analysis process, which is usually based on the extraction of the optical phase distribution encoded by the generated correlation fringes. From these data, in-plane displacement fields can be measured over the whole surface of any rough object without making contact with it. Unwrapped phase distribution is useful because it allows direct whole field evaluations of residual stresses [7,8].

In this paper, deformations of the base metal and welding part of butt-welded specimens are measured by using in-plane displacement sensitive ESPI. Young's modulus of base metal and the welding zone are determined from the result of ESPI. The residual stress distribution of butt-welded specimens can also be estimated from the strain profile of ESPI and Young's moduli. This is contrasted with other analysis methods. The presented method offers an improved speed of evaluation due to the elimination of the surface preparation time of the hole-drilling technique.

2. Materials and methods

2.1. ESPI

Laser has high coherence characteristics as two or more waves can be interfered in the coherence length. When an optically rough surface of an object is illuminated by a coherent laser beam, the beam is scattered in all directions. These scattered laser beams are interfered by each other and the intensity of each point on an image obtained by a charge-coupled device camera varies randomly. This phenomenon is well known as the speckle effect. ESPI measurement using a laser uses this speckle phenomenon so that the displacement of an object by the deformation can be measured.

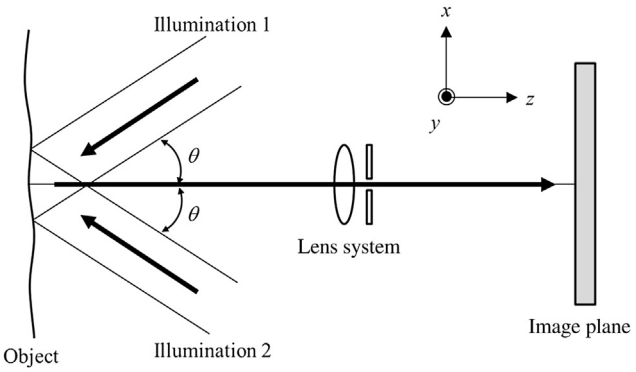

Fig. 1 – Schematic of in-plane displacement sensitive interferometer.

Fig. 1 shows a schematic of an in-plane displacement sensitive interferometer. Two laser beams are illuminated with the same angle θ on the surface of an object at the same time. Illuminated beams form the speckle pattern on the surface of an object, and these speckle patterns are interfered to form another speckle pattern. This pattern is formed by the phase difference of illuminated beams. When the path of the laser beam can be traced, the relationship between the laser beam and the phase can be shown as follows:

$$\Delta\phi = \delta_1 - \delta_2 = \frac{4\pi}{\lambda} d_x \sin\theta_i \quad (1)$$

where: δ_1 = optical path length of beam 1; δ_2 = optical path length of beam 2; λ = wavelength of a laser; d_x = x-axis component of sensitivity vector d; and θ_i = angle between illumination direction and normal direction to surface.

The path of a laser beam between the laser source and the image plane or charge-coupled device camera in one direction is shown in Fig. 2. In Fig. 2, d is the sensitivity vector of this interferometer and θ_i is the angle between the illumination direction and the normal direction to the surface of an object; θ_d the angle between the sensitivity vector and the normal direction to the surface of an object, and θ_v an angle between the viewing direction and the normal direction to the surface of an object. As an interference fringe pattern is formed by δ_1 and δ_2, the optical path lengths of the two beams and the phase difference can be written as Equation 1.

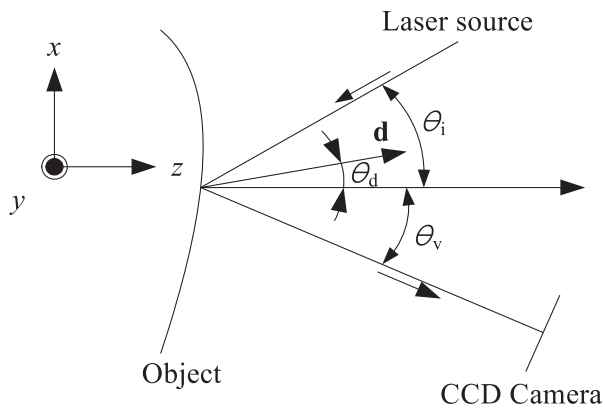

Fig. 2 – Optical path difference as the object deformation.

Therefore, the z-axis component of the sensitivity vector d in an in-plane displacement sensitive interferometer is eliminated and only d_x can be measured when the phase difference is obtained. This phase difference can be calculated with a phase shifting method. The intensity of image resulting from the interference of two beams is written as Equation 2.

$$I(x,y) = I_1(x,y) + I_2(x,y) + 2\sqrt{I_1(x,y)I_2(x,y)\cos\phi(x,y)} \quad (2)$$

where: I = intensity distribution of interference image; I_1 = intensity distribution of beam 1; I_2 = intensity distribution of beam 2; and ϕ = phase distribution of interference image.

In order to calculate the phase at each pixel on an interference image, the four-step phase shifting method is generally employed [9]. For shifting the phase, a piezoelectric transducer (PZT) is used and the step movement amount of the phase is $\pi/2$. If the intensity distributions of four phase-shifted interference images when an object is in the steady state are I_1, I_2, I_3, and I_4, then the phase distribution of an object surface can be obtained from Equation 3.

$$\phi = \tan^{-1}\left[\frac{I_4 - I_2}{I_1 - I_3}\right] \quad (3)$$

Similarly, because the intensity distributions of four phase-shifted interference images have the phase deference $\Delta\phi$, the phase distribution of an object after deformation is $\phi + \Delta\phi$, and finally $\Delta\phi$, the phase deference due to the deformation can be calculated by subtracting the phase distribution prior to the deformation from the phase distribution after the deformation.

2.2. Residual stress calculation

For this calculation, it was assumed that the distribution of residual stresses included in the heat-affected zone and welding part are the same.

From the general tensile loading testing for a standard specimen using UTM (universal testing machine), Young's modulus of base metal E_b is obtained. By Hooke's law, the relationship between stress σ_b and strain ϵ_b is defined as Equation 4.

$$\sigma_b = E_b \cdot \epsilon_b \quad (4)$$

With Equation 4, the stress of the base metal can be obtained and for the welded specimen, residual stress included in the welded area σ_R has to be concerned as follows:

$$\sigma_R + \sigma_b = E_w \cdot \epsilon_w \quad (5)$$

where: E_w = Young's modulus of butt-welded part; ϵ_w = strain of butt-welded part; and σ_b = stress of base metal part.

When Equation 4 substitutes for Equation 5, Equation 6 is derived. Therefore the residual stress can be calculated from Equation 6 directly.

$$\sigma_R = E_w \cdot \epsilon_w - E_b \cdot \epsilon_b \quad (6)$$

where: E_w = Young's modulus of butt-welded part; ϵ_w = strain of butt-welded part; E_b = Young's modulus of base metal part; and ϵ_b = strain of base metal part.

Using ESPI, the deformation of the base metal and the welded part in a specimen can be measured. From the result of ESPI, E_w, E_b, ϵ_w, and ϵ_b are calculated so that the residual stress σ_R is obtained. Therefore, with this suggested method, the residual stress of a butt-welded part can be calculated quantitatively, unlike any other optical methods, with a hole drilling method [10,11].

2.3. Numerical analysis

Finite element method is a useful method to simulate the behavior of components or a structure. Finite element method is also used as a comparison tool. To analyze the behavior of a component, the model of a component should

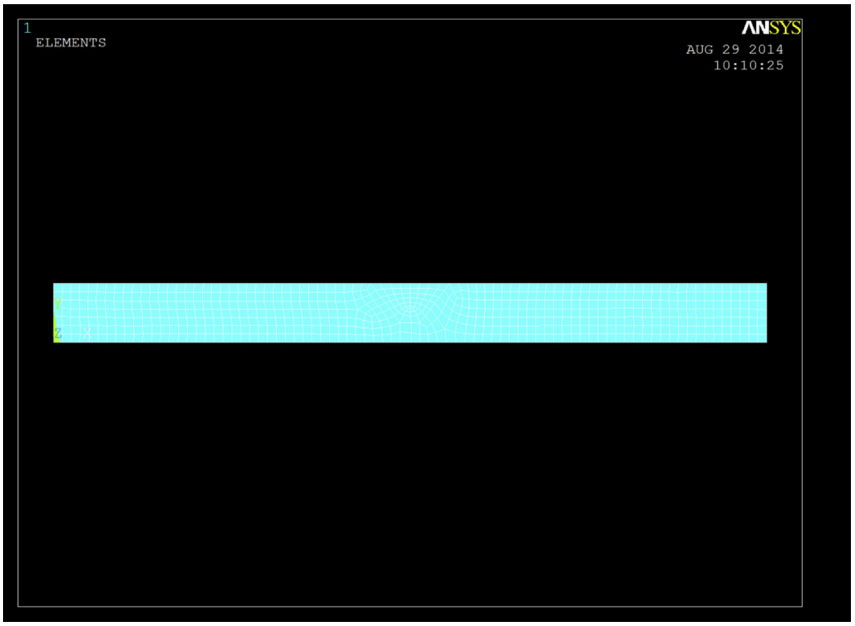

Fig. 3 – Element and mesh of specimen for numerical analysis with ANSYS.

Table 1 – Mechanical properties of ASTM A36.

Properties	Specification
Material	ASTM A36
Young's modulus	210 GPa
Poisson's ratio	0.26
Density	7,850 kg/m^3

Table 2 – Physical properties of ASTM A36.

Properties	Specification
Specific heat (J/kg·K, at 20 °C)	470
Resistivity (μΩ·cm)	17.0
Thermal conductivity (W/m·K, at 100 °C)	52.0

Table 3 – Thermal expansion coefficient of ASTM A36.

Temperature (°C)	CTE (10^{-6}/°C)
30	12.8
700	15.2
850	11.9
900	12.1
1,000	13.0
1,200	14.3
1,500	15.2

first be created with internal or external modeling tools in the proper analysis method such as structural, thermal, etc. Some material properties of a target material should then be provided. The constraint and force conditions are applied on the model. Finally, the behavior of a created model can be solved.

For analyzing the residual stress included in a component, more complicated analysis is required. With a created model, the heat transfer analysis is done at first. Some parameters obtained from the result of this analysis are used in the thermo-elasto-plastic analysis. This is known as a thermal–structural coupled analysis.

In this paper, for the comparison of results, a commercial tool, ANSYS (stands for Analysis System, ANSYS Inc., Canonsburg, PA, USA) version 13 was used as a numerical analysis tool. In order to analyze the residual stress of the butt-welded part of a specimen, the heat transfer analysis with PLANE55 element, which is a quadrilateral element type, should first be selected in order to acquire the thermal stresses. Its result is then used as a load parameter for structural analysis with PLANE42 element type which is also a quadrilateral element. The size of an element is inputted with 0.005/2. The meshed shape of specimen is as shown in Fig. 3. The material properties, physical properties, and coefficient of thermal expansion those are used for solving the residual stress are as shown in Tables 1–3.

2.4. *Experiment*

Carbon structural steel (ASTM A36) with a thickness of 6.0 mm was butt welded. For this experiment, the butt-welding process with CO_2 welding was employed. In order to measure the residual stresses due to the amount of heat created by the welding process, the welding process was carried out with welding current of 130 A, 140 A, and 150 A, respectively, and the feed speed was 2 mm/s. The root gap between plates was 1 mm, the groove angle was 60°, and the depth of groove was 4 mm. To minimize the effect of deformation such as compression and torsion during welding, both plates were fixed with jig on the automatic welding system as shown in Fig. 4 and the butt-welded plate was cooled down slowly.

Butt-welded standard tensile testing specimens [12] were prepared to measure stress distribution around the welded part. The specimen was cut by using the electric discharge machining method. Two types of specimen were fabricated as shown in Fig. 5. Type I was made of the base metal part and Type II includes the butt-welded part. The specimen had an overall length of 200 mm, gage length of 50 mm, width of 10 mm, and a radius of fillet of 20 mm. Mechanical

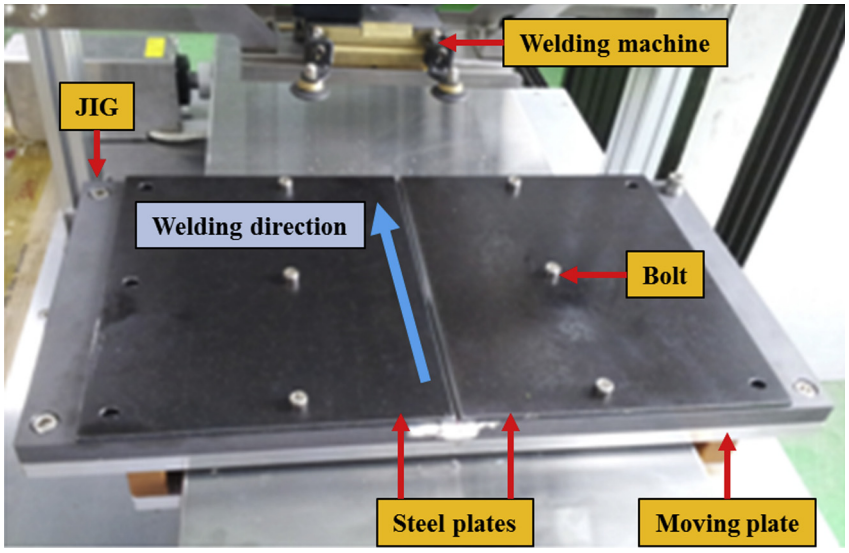

Fig. 4 – Automatic welding system is consists of welding machine, moving plate, and JIG.

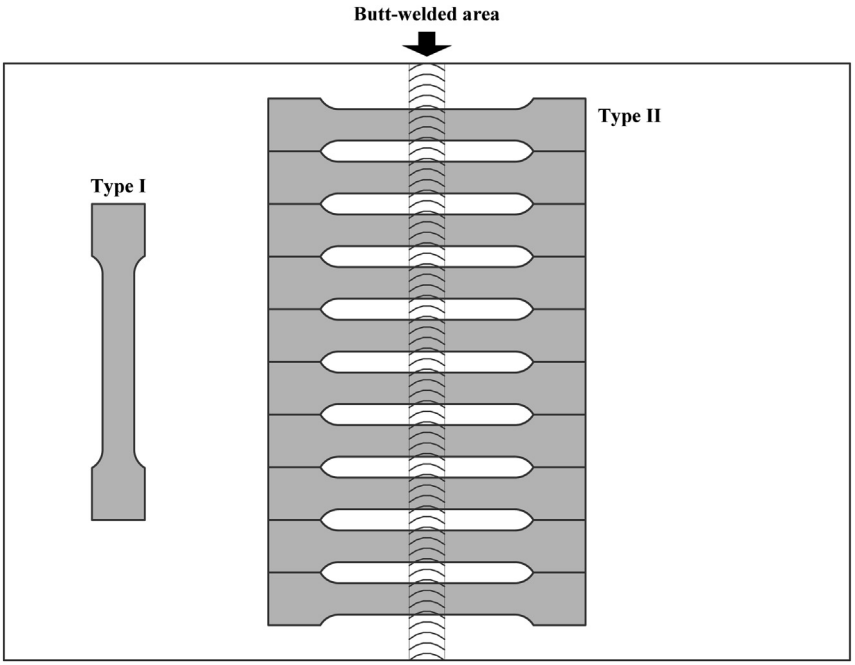

Fig. 5 – Fabrication of specimen for tensile testing.

and physical properties and the coefficient of thermal expansion of a specimen are as shown in Tables 1–3.

As shown in Fig. 6, a material test system (Landmark system 370.10) was used for tensile testing to measure both the deformations and Young's moduli of the base metal and welded specimens. At first, a base metal specimen was tested to find the range of elastic bandwidth of A36 material. With this test, the stress-strain curve was taken as shown in Fig. 7. Each tensile test of a specimen including the welded part was then done in the range of elastic bandwidth. During the tensile testing, forces of 3 kN, 4 kN, and 5 kN were each loaded for 30 seconds. Using the ESPI system (Q300; Dantec Dynamics, Skovlunde, Denmark), the deformation of specimen was obtained so that the strain variation and stress distribution due to the increment of the tensile loading was calculated. To eliminate environmental disturbance, the ESPI system connected to the tripod was set on the optical table with an isolator. Each test was performed more than three times. The configuration of the experimental setup is shown in Fig. 6. The phase map images of each tensile loading step were obtained manually when the interference fringe pattern was in the stable state.

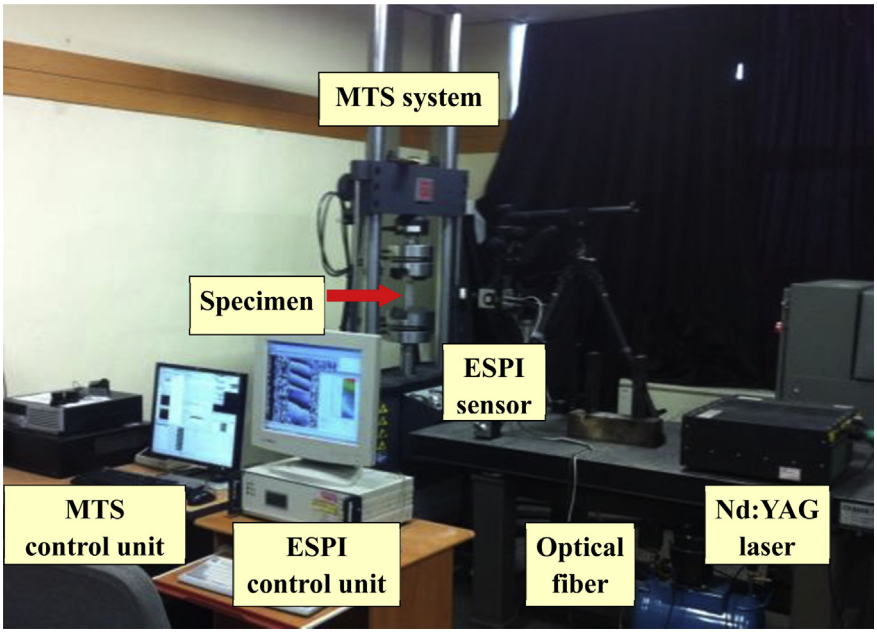

Fig. 6 – Experimental setup of tensile testing with electronic speckle pattern interferometry system.

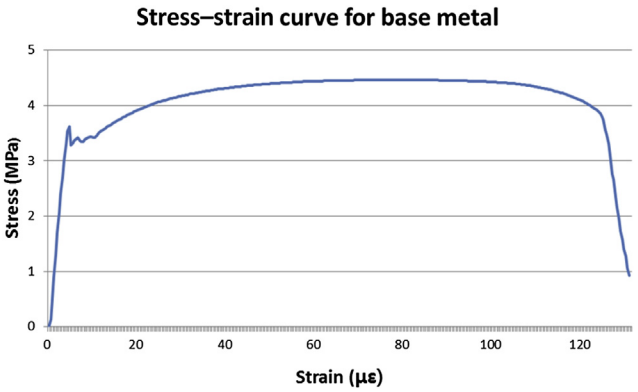

Fig. 7 – Stress–strain curve for base metal obtained by tensile testing.

Tables 4–6 show the phase map results of the experiment due to the tensile loading difference at each welding current condition. Phase map images were converted to the unwrapped image to analyze the deformation quantitatively. With these unwrapped results, the displacement values of each pixel along the center line of a specimen in the tensile loading direction were obtained as shown in Tables 7–9. Using Equations 4–6, strain, Young's moduli, and stress of the base metal part and welded part were calculated. For all numerical calculations, only the welded part was considered when calculating the residual stress.

3. Results

As shown in Tables 4–6, the number of interference fringe was increased when the tensile loading force difference was increased. However, the height between the interference fringes of the welded part in the tensile loading direction was slightly different from that of the base metal. From this result, it is estimated that the material property at the welded part was changed. In Tables 4–6, the slope of interference fringes was inclined by a small amount. This is significant because the specimen was grabbed unevenly by the grip of the material test system. Figs. 8–10 show profile data and we can see that the deformation value of the welded part is smaller than that of the base metal part. When the tensile loading force is

Table 5 – Phase map due to the tensile loading difference at welding current of 140 A using electronic speckle pattern interferometry.

Welding current (A)	140		
Tensile loading (kN)	3	4	5
Phase map	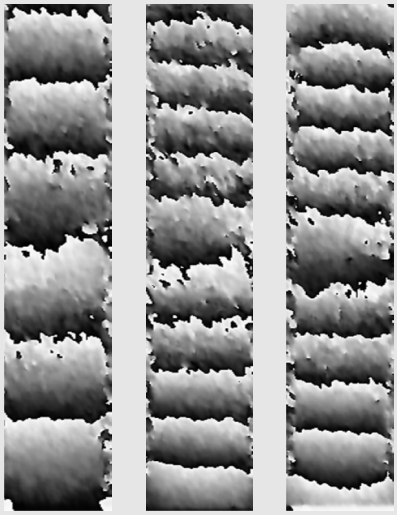		

Table 4 – Phase map due to the tensile loading difference at welding current of 130 A using electronic speckle pattern interferometry.

Welding current (A)	130		
Tensile loading (kN)	3	4	5
Phase map	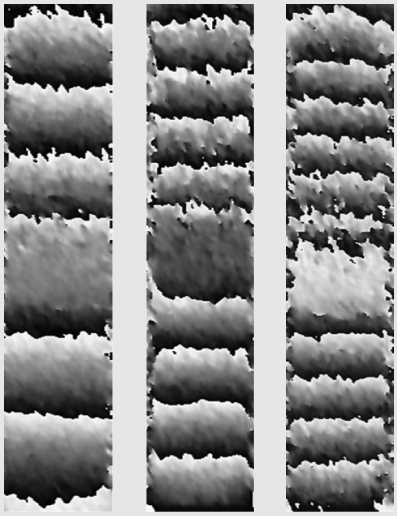		

Table 6 – Phase map due to the tensile loading difference at welding current of 150 A using electronic speckle pattern interferometry.

Welding current (A)	150		
Tensile loading (kN)	3	4	5
Phase map	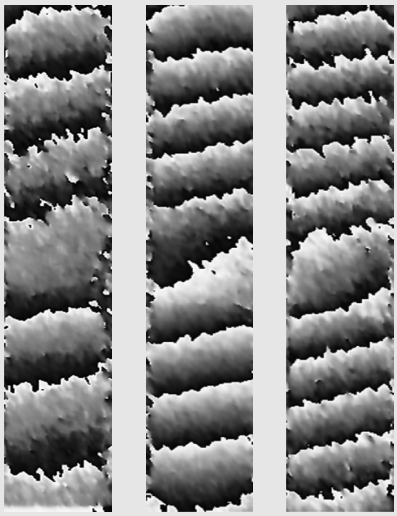		

Table 7 – Phase map due to the tensile loading difference at welding current of 150 A using electronic speckle pattern interferometry.

Welding current (A)	130		
Tensile loading (kN)	3	4	5
Line profile	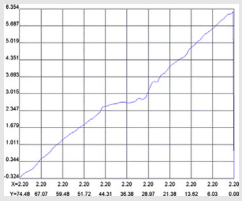	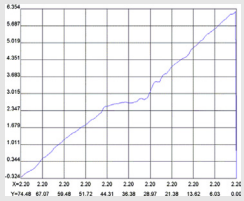	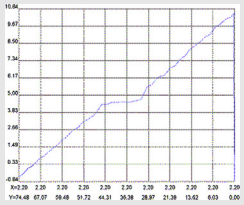

Table 8 – Phase map due to the tensile loading difference at welding current of 150 A using electronic speckle pattern interferometry.

Welding current (A)	140		
Tensile loading (kN)	3	4	5
Line profile	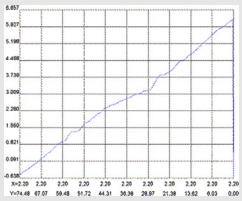	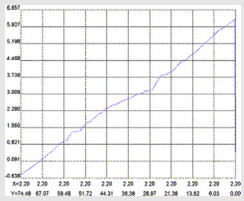	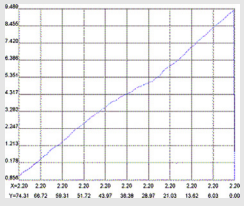

Table 9 – Phase map due to the tensile loading difference at welding current of 150 A using electronic speckle pattern interferometry.

Welding current (A)	150		
Tensile loading (kN)	3	4	5
Line profile	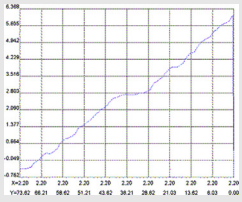	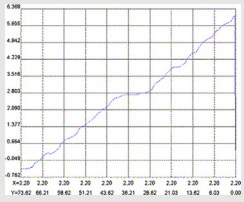	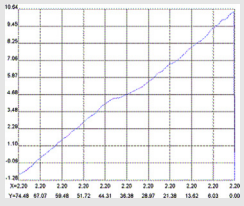

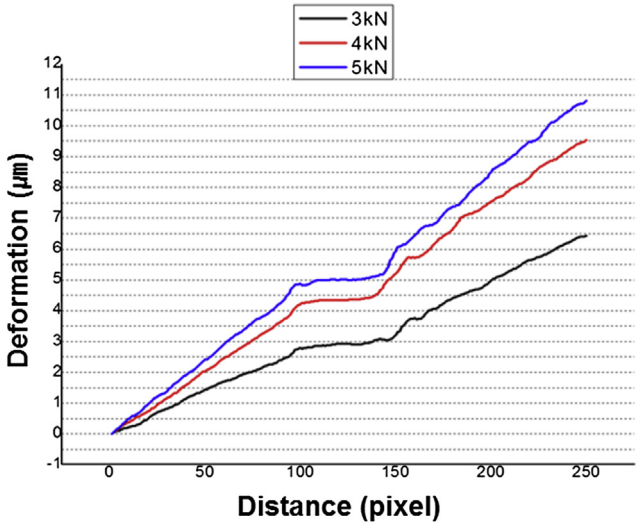

Fig. 8 – Deformation distribution along the center line of specimen in tensile loading direction (welding current 130A).

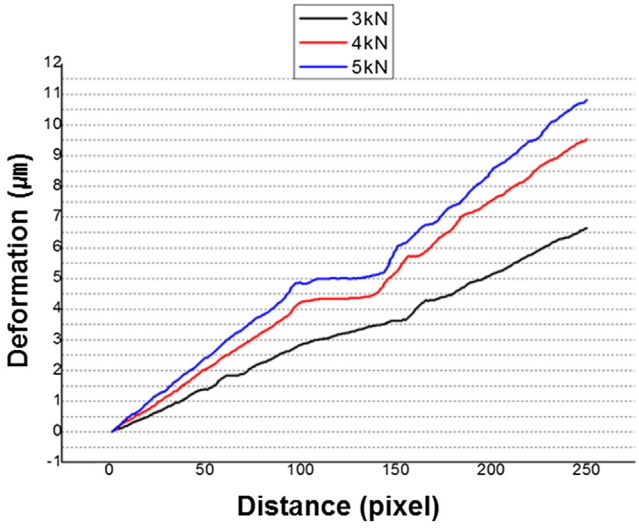

Fig. 9 – Deformation distribution along the center line of specimen in tensile loading direction (welding current 140A).

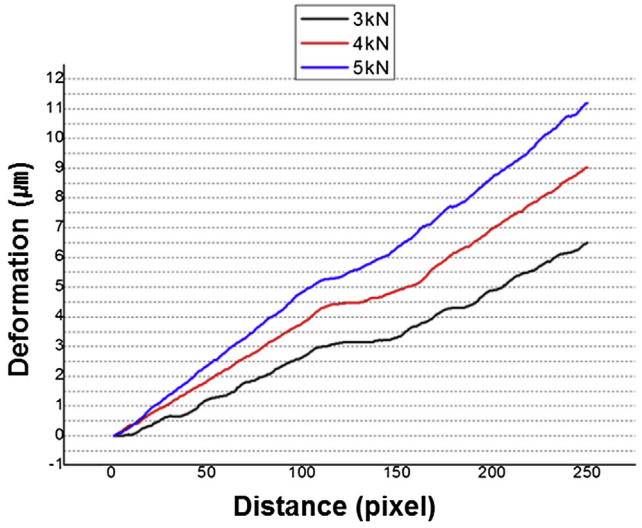

Fig. 10 – Deformation distribution along the center line of specimen in tensile loading direction (welding current 150A).

increased, the slope of the deformation distribution line is also increased.

From the line profile results, the strain distribution was obtained along the center line of the specimen in the tensile loading direction. Using the strain distribution, Young's moduli of the base metal and welded part were calculated numerically because the cross sectional area of specimen and the tensile loading force are known values, Tables 10–12 show the results of the numerical calculations for each welding current condition. Finally, by using Equations 4–6, the residual stress remained in the welded part after the specimen was fabricated by the electric discharge machining method was obtained by using ESPI system only as shown in Table 13. From the results, it was confirmed that when the welding current and the tensile loading are increased, then the residual stresses remaining in the welded part also increase. In Table 13, the residual stress values are all negative. This means that when the tensile loading is applied to the specimen, the welded part is compressed.

Table 10 – Results of numerical calculation in case of welding current of 130 A.

Tensile loading (kN)		3	4	5
Base metal	Cross-sectional area (m^2)	7.50E-05	7.50E-05	7.50E-05
	Stress (MPa)	4.00E+07	5.33E+07	6.67E+07
	Deformation (μm)	1.09E+01	1.45E+01	1.81E+01
	Strain	1.91E-04	2.54E-04	3.18E-04
	Young's modulus (GPa)	2.09E+11	2.10E+11	2.09E+11
Weld part	Cross sectional (m^2)	8.78E-05	8.78E-05	8.78E-05
	Stress (MPa)	3.42E+07	4.56E+07	5.69E+07
	Deformation (μm)	6.42E+00	1.00E+01	1.12E+01
	Strain	1.37E-04	2.14E-04	2.39E-04
	Young's modulus (GPa)	2.50E+11	2.13E+11	2.38E+11

Table 11 – Results of numerical calculation in case of welding current of 140 A.

Tensile loading (kN)		3	4	5
Base metal	Cross sectional area (m^2)	7.50E-05	7.50E-05	7.50E-05
	Stress (MPa)	4.00E+07	5.33E+07	6.67E+07
	Deformation (μm)	1.07E+01	1.43E+01	1.78E+01
	Strain	1.91E-04	2.55E-04	3.18E-04
	Young's modulus (GPa)	2.09E+11	2.09E+11	2.10E+11
Weld part	Cross sectional (m^2)	9.58E-05	9.58E-05	9.58E-05
	Stress (MPa)	3.13E+07	4.18E+07	5.22E+07
	Deformation (μm)	6.63E+00	9.53E+00	1.09E+01
	Strain	1.38E-04	1.99E-04	2.27E-04
	Young's modulus (GPa)	2.26E+11	2.10E+11	2.30E+11

For the comparison of the residual stress measured by using the ESPI system, a numerical analysis using ANSYS was used. From the result of a numerical analysis, the maximum residual stress of the welding part whose welding current is 130 A and tensile loading is 3 kN, was −6.295 MPa as shown in Fig. 11. The error between these results is about 7.39%. It seems that the residual stress decreased because of the fabrication process of the specimen. Figs. 11–13 show the analysis results of the residual stress for all of the welding and tensile loading conditions. The results of the numerical analysis are shown in Table 14. Table 15 shows the deviation rates between the results of ESPI experiment and ANSYS analysis. It was confirmed that the result of the ESPI

Table 12 – Results of numerical calculation in case of welding current of 150 A.

Tensile loading [kN]		3	4	5
Base metal	Cross sectional area (m^2)	7.50E-05	7.50E-05	7.50E-05
	Stress (MPa)	4.00E+07	5.33E+07	6.67E+07
	Deformation (μm)	1.05E+01	1.40E+01	1.75E+01
	Strain	1.91E-04	2.55E-04	3.18E-04
	Young's modulus (GPa)	2.09E+11	2.10E+11	2.09E+11
Weld part	Cross sectional (m^2)	1.06E-04	1.06E-04	1.06E-04
	Stress (MPa)	2.84E+07	3.79E+07	4.74E+07
	Deformation (μm)	6.49E+00	9.03E+00	9.96E+00
	Strain	1.30E-04	1.81E-04	1.99E-04
	Young's modulus (GPa)	2.19E+11	2.10E+11	2.38E+11

Table 13 – Residual stresses (MPa) remained in the welding part of each specimen measured using electronic speckle pattern interferometry system.

Welding current (A)	Tensile loading (kN)		
	3	4	5
130	−5.83	−7.78	−9.72
140	−8.68	−11.6	−14.5
150	−11.6	−15.4	−19.3

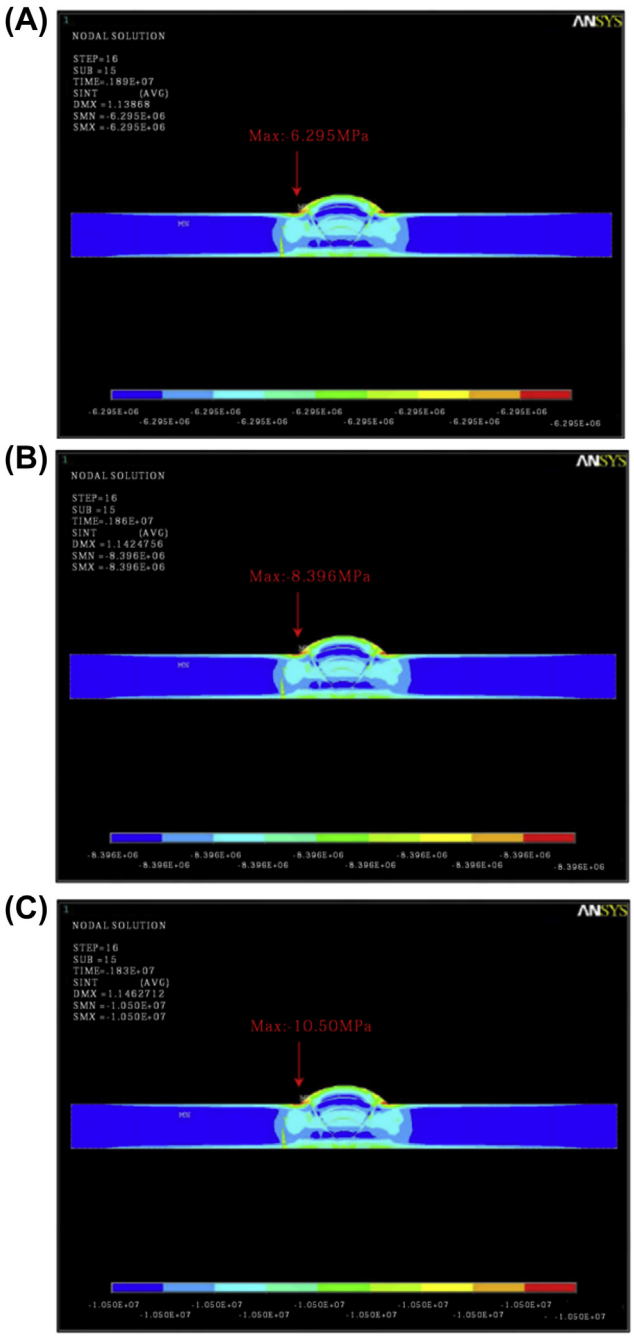

Fig. 11 – Residual stress of the welding part obtained by numerical analysis (Welding current: 130A). (A) 3 kN, (B) 4 kN, and (C) 5 kN of tensile loading condition.

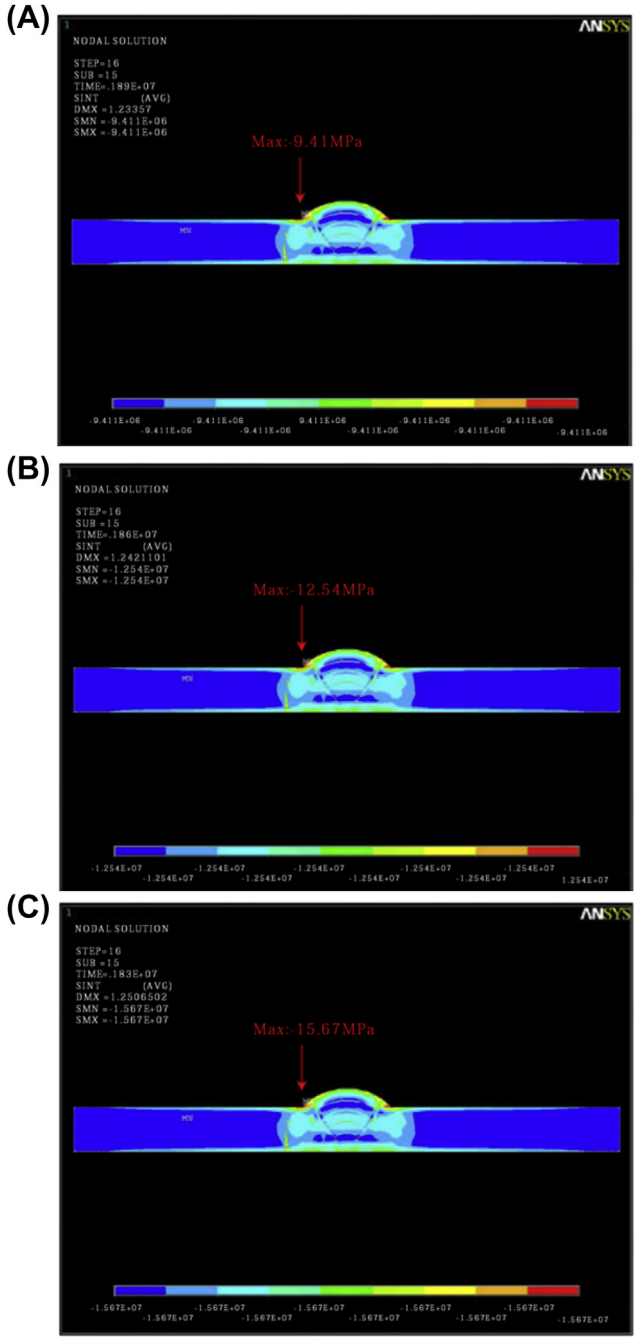

Fig. 12 – Residual stress of the welding part obtained by numerical analysis (Welding current: 140A). (A) 3 kN, (B) 4 kN, and (C) 5 kN of tensile loading condition.

experiment is in good agreement with that of the ANSYS analysis. The average of the deviation rates is 7.48%.

In conclusion, a new residual stress measurement technique using the ESPI system with a material test machine was suggested. This technique was applied to measure the residual stress of the welded part of a specimen. Young's moduli of the base metal and welding part of ASTM A36 specimen were measured as 210 Gpa and 201–250 GPa, respectively. From the result, it was experimentally confirmed that the residual stress acts constantly in the welding part. The stress and the strain along the center line in tensile loading direction of the specimen were measured quantitatively. The strain of the base metal and the welded part was linearly increased when the tensile loading was increased. The residual stresses of the welding part of the ASTM A36 specimen that was welded with the welding current of 130 A were 5.83 MPa, 7.78 MPa, and

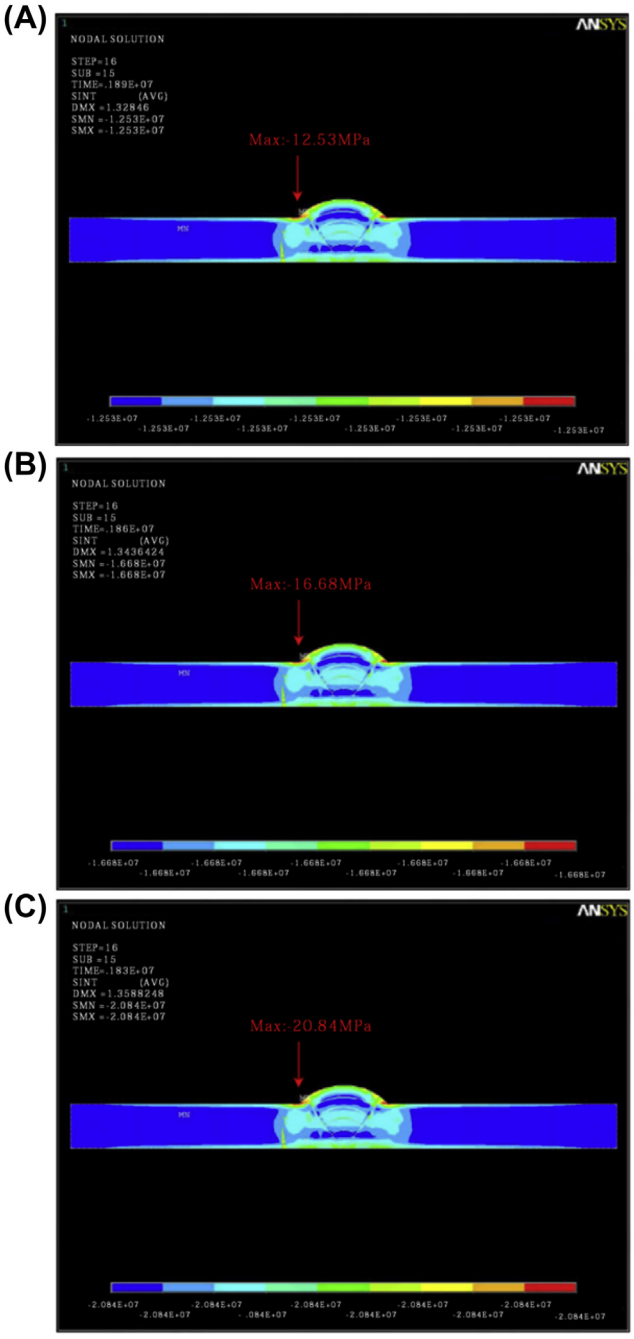

Fig. 13 – Residual stress of the welding part obtained by numerical analysis (Welding current: 150A). (A) 3 kN, (B) 4 kN, and (C) 5 kN of tensile loading condition.

9.72 MPa. For the welding current of 140 A, these were 8.68 MPa, 11.6 MPa, and 14.5 MPa and for the welding current of 150 A they were 11.6 MPa, 15.4 MPa, and 19.3 MPa with negative sign. Therefore, this shows that ESPI without the hole-drilling method can be used as a very useful method to measure the residual stress of a welded components or a structure.

Table 14 – Residual stresses (MPa) remained in the welding part of each specimen analyzed using ANSYS.

Welding current (A)	Tensile loading (kN)		
	3	4	5
130	−6.30	−8.40	−10.5
140	−9.41	−12.5	−15.7
150	−12.5	−16.7	−20.8

Table 15 – Deviation rates of residual stresses (%) obtained using electronic speckle pattern interferometry system and ANSYS analysis.

Welding current (A)	Tensile loading (kN)		
	3	4	5
130	7.39	7.34	7.43
140	7.76	7.50	7.47
150	7.42	7.67	7.39

Conflicts of interest

All contributing authors declare no conflicts of interest.

Acknowledgments

This work was supported by the International Collaboration R&D Program through the Korea Institute for Advancement of Technology Grant funded by the Ministry of Knowledge Economy (Grant No. N0000682), South Korea and was also supported by a Nuclear Research & Development Program of the National Research Foundation of Korea (NRF) grant funded by the Korean government (MSIP), (Grant No. 2012M2B2B1055611).

REFERENCES

[1] J. Lu, Handbook on Residual Stress, in: Residual Stress: Manufacturing and Materials Processing, Society for Experimental Mechanics, second ed., vol. 1, 2005 xiii–xxiv.
[2] C. Weisman, Welding Handbook, seventh ed., American Welding Society, 1976, pp. 222–268.
[3] V. Ramamurti, S. Suresh, B. Raghuraman, G. Ravichandran, Residual stress analysis in weldments, Eng. Fract. Mech. 38 (1991) 385–391.
[4] G. Schajer, Practical Residual Stress Measurement Methods, John Wiley & Sons, London, 2013.
[5] G. Cloud, Optical Methods of Engineering Analysis, Cambridge University Press, Cambridge, 1990, pp. 453–491.
[6] K.S. Kim, H.C. Jung, K.S. Kang, J.K. Lee, S.S. Jarng, C.K. Hong, In-plane strains measurement by using the electronic speckle pattern interferometry, KSME Int. J. 12 (1998) 215–222.
[7] E. Ponslet, M. Steinzig, Residual stress measurement using the hole drilling method and laser speckle interferometry, part II: analysis technique, Exp. Tech. 27 (2003) 17–21.
[8] G. Schajer, M. Steinzig, Full-field calculation of hole drilling residual stresses from electronic speckle pattern interferometry data, Exp. Mech. 45 (2005) 526–532.
[9] K. Creath, Phase-shifting speckle interferometry, Appl. Opt. 24 (1985) 3053–3058.

[10] X. Huang, Z. Liu, X. Huimin, Recent progress in residual stress measurement techniques, Acta Mech. Solida Sin. 26 (2013) 570–583.
[11] N.S. Rossini, M. Dassiti, K.Y. Benyounis, A.G. Olabi, Methods of measuring residual stresses in components, Mater. Des. 35 (2012) 572–588.
[12] Standard Test Methods and Definitions for Mechanical Testing of Steel Products, Designation: A370-05, Annual Book of ASTM Standards, vol. 2006, 2006, pp. 87–133, 01.03.